DC Bias Impact on Magnetic Core Losses at High Frequency

Bima Nugraha Sanusi and Ziwei Ouyang
DTU Electro, Technical University of Denmark (DTU)
Kongens Lyngby, Denmark
Email: bnusa@elektro.dtu.dk
URL: https://www.ele.elektro.dtu.dk

Keywords

≪Core loss≫, ≪Core Loss Modeling≫, ≪Magnetic Device≫.

Abstract

This paper aims to provide more insight into core losses at high frequency (MHz range) with superimposed DC bias in ferrite. Inductive cancellation method is employed to reduce measurement sensitivity to phase errors. The tested MnZn ferrite has a nominal relative permeability (μ_r) of 1500 (core A) and 800 (core B), which was tested at frequency from 500 kHz to 3 MHz. The DC bias appears to create a shift in the Steinmetz parameters, in particular the k_i and β are affected the most. Higher B_{DC} creates higher losses gain and higher f_{sw} makes the relative losses increase lower. This is a new finding. Furthermore, the Steinmetz Premagnetization Graph (SPG) with iGSE method ise used to create a core losses prediction model. A maximum error of 25% were found. The measurement data and the built model will be published online for use by other magnetics designer.

1 Introduction

It is increasingly necessary to know core losses with reasonable accuracy in the intended application. This is to avoid overheating on the one hand and oversizing on the other. There are 2 steps in knowing the core losses. The first is measuring the core losses to know the behaviour of the core. The second is modeling the core losses to predict what losses are going to occur under a certain condition. The designer may skip the first step by relying on the published core losses data from the manufacturer. However, the intended application may have different core geometry, excitation waveform, and operating condition than the published data. This will have an impact on the core losses prediction accuracy. The modeling stage aims to predict the core losses based on a set of measurement data. With accurate measurement and modeling, the designer can find the optimal point in the magnetic component design.

There are numerous ways to model the magnetic core losses. They can be classified as the following.

- Hysteresis loop based: the dissipated energy per cycle is determined from the hysteresis loop area. The Preisach [1] and Jiles-Atherton models are examples of this. The approach is accurate but requires many parameters and accurate hysteresis loop measurement.
- Steinmetz Equation (SE) based: core losses per volume is modeled by the power equation. From there stems various models [2, 3, 4], which attempt to improve the loss prediction accuracy under different excitation.
- Loss separation based: the total power losses are constructed by calculating separately the hysteresis loss and eddy current loss and summing them. The calculation uses basic core geometry and material properties, such as conductivity and coercivity. This approach was demonstrated in [5, 6]. It is useful when extensive measurement data is not available.

The SE based model is the most adopted approach by magnetics designer. This is due to the practicality of power formulae. However, measurement data is necessary for this approach.

Core loss measurement techniques can be classified into calorimetric and electric method. Calorimetric method works based on the energy conservation law. The core losses creates heat. The heat is measured in the form of temperature rise. From temperature rise and thermal properties, the core losses can be estimated. This method is well known. A recent work [7] uses the transient principle to reduce measurement time. The major drawback of this method is the difficulty to separate winding loss. Electric method does not have this drawback. It works by measuring induced voltage and excitation current. The induced voltage measurement automatically excludes the winding losses. Therefore, this method is chosen in this paper.

Methods such as [8, 4, 9] can be used to predict core losses with any excitation waveform. However, their validity needs to be re-investigated. Those models work under the assumption of non-changing Steinmetz parameters. Unfortunately, the Steinmetz parameters can change at higher frequency [10] or in the presence of DC bias [11, 12]. There is also a missing experimental verification for core losses under square wave excitation at higher frequency. Recent reports in [7, 13] measure losses only under sine wave excitation. The authors in [14, 15] measure losses with square wave excitation only up to 500 kHz. Therefore, this paper aims to provide more insight to core losses by providing more measurement results.

The focus of the present work is to investigate magnetic core losses under square wave excitation with DC bias. The frequency of interest is up to 3 MHz. The DC bias impact will be quantified and the current core losses model will be extended or modified to incorporate the impact. Behaviour in different core material and geometry is also investigated. Through the end, we will see if the current losses model still matches experimental measurement. The parameter shift will also be analyzed.

2 Core Losses Measurement Setup

Measurement Principle

The main difficulty in measuring core losses with electric method is that ferrites generally have low losses compared to the stored energy. This creates the phase angle ϕ between v_{DUT} and i (illustrated in Fig. 1) close to 90°, since the impedance of magnetizing inductor $L_{\mathrm{m,DUT}}$ is much smaller than the equivalent core loss resistor $R_{\mathrm{Fe,DUT}}$. The relative power error caused by the phase discrepancy $\Delta\phi$ for sinusoidal excitation is given by (1), which was derived in [16]. It is virtually impossible to eliminate $\Delta\phi$ in an actual measurement setup. Therefore, a more effective solution to limit the power error is to control $tan(\phi)$.

$$\left|\frac{\Delta P}{P}\right| = |tan(\phi)| \cdot |\Delta\phi| \tag{1}$$

The mutual inductance neutralization [17] or inductive cancellation [18] technique can bring $tan(\phi)$ to a more feasible region. However, this method requires a very accurate compensating inductance or capacitance. This is not easy to design. A more recent improvement of this cancellation concept [14] allows less strict compensation requirement. This is called partial cancellation concept and is done by introducing the cancellation factor k. The same concept is adopted in this work.

The core losses measurement circuit is shown in Fig. 1. R_{p} and L_{p} represent the winding resistance and stray inductance, respectively, on the primary side. On the secondary side, they are represented by R_{s} and L_{s}. L_{m} is the magnetizing inductance. A DC blocking capacitance C_{DC} is necessary to avoid saturation in the magnetic core. Current sensing is done by measuring voltage across the resistor R_{sense}. However, due to component nonideality, a parasitic inductance L_{sense} will also be present. As the focus of this work is square wave excitation, a half bridge is used to generate it. A controllable DC current source I_{DC} is also used to generate the DC bias, which is also an important part of this work. Parasitic capacitances from measurement devices are shown by C_{probe} and C_{diff}. It is worth mentioning that for measuring low

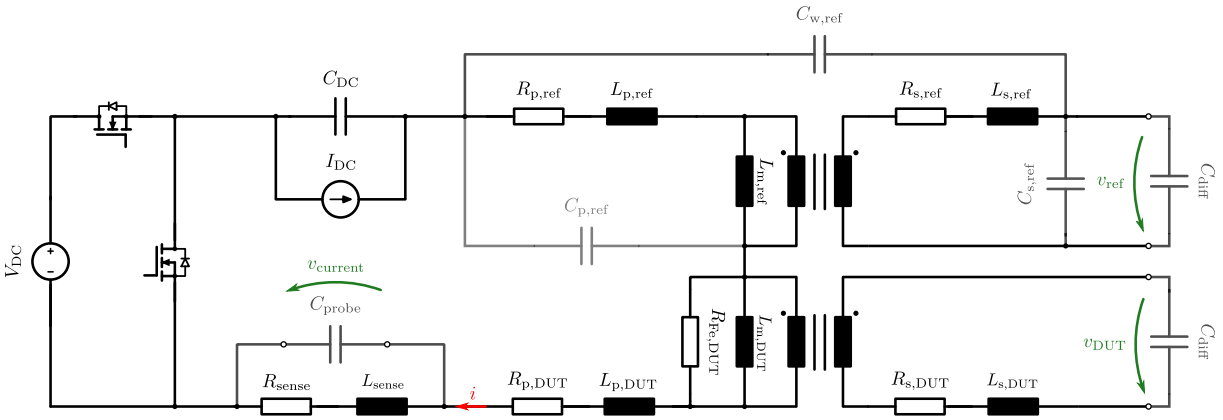

Fig. 1: Electrical circuit of the core losses measurement system. *DUT* means the magnetic device under test and *ref* means the reference / compensation element. Magnetic core losses is represented by $R_{\mathrm{Fe,DUT}}$

losses core, it is difficult to find a magnetic core with much negligible core losses, compared to *DUT*. Therefore, we chose to make the reference element by air core inductor which does not have core losses.

Based on the measurement circuit, the core losses can be calculated by (2), where T_{sw} is the waveform period. For a square wave excitation, the cancellation factor k is calculated by (3). This factor represents the percentage of cancelled reactive voltage to the total reactive voltage. The partial cancellation mechanism creates a virtual voltage $v_{\mathrm{comp}} = v_{\mathrm{DUT}} - v_{\mathrm{ref}}/k$ to replace the initial v_{DUT}. As a result, the phase shift between v_{comp} and measured current can be kept minimum, even when the reference element value $L_{\mathrm{m,ref}}$ has a mismatch with $L_{\mathrm{m,DUT}}$. Therefore, the measurement error can be minimized.

$$P_{\mathrm{Fe}} = \frac{1}{T_{\mathrm{sw}}} \left(\int_0^{T_{\mathrm{sw}}} v_{\mathrm{DUT}} \cdot i_{\mathrm{meas}}\, dt - \frac{1}{k} \int_0^{T_{\mathrm{sw}}} v_{\mathrm{ref}} \cdot i_{\mathrm{meas}}\, dt \right) \tag{2}$$

$$k = \frac{V_{\mathrm{ref,pp}}}{V_{\mathrm{DUT,pp}}} \tag{3}$$

Voltage Measurement

Differential voltage probes are used for the voltage measurement because of the floating measuring position. We chose 25 MHz active differential probe from Testec, which should provide enough bandwidth for 3 MHz square waveform. An additional benefit of the differential probe is the low parasitic capacitance. In this case, it has an equivalent capacitance of 2.75 pF, which is lower compared to 10 pF of common passive probes. One typical drawback is the measurement delay and rise time. Therefore, the differential probes are calibrated to generate identical waveform as measured by a 200 MHz passive probe, before any measurements are performed. A comparison of the waveforms is shown in Fig. 2. The post-processing step will compensate the time delay based on the calibration data.

Voltage measurements (v_{ref} and v_{DUT}) are influenced by the parasitic capacitances. In the DUT, intra and inter-winding capacitances are minimized by using only 1 turn for primary and secondary winding, and keeping enough distance between both windings. Therefore, DUT's parasitic capacitances are neglected in this work. The reference air core needs more winding turns and close distance between primary and secondary. It makes the parasitic capacitances non-negligible. In particular, $C_{\mathrm{w,ref}}$ and $C_{\mathrm{s,ref}}$ will influence the voltage reading. Those capacitances cause extra current flow which makes a voltage drop on secondary $R_{\mathrm{s,ref}}$. This voltage drop is included in the voltage measurement and affect the power calculation.

The formulas given in [14] are used to quantify to potential error. The errors from reference core inter-winding and intra-winding capacitances are given in (4) and (5) respectively. The error from DUT side, caused by voltage probe capacitance, is given in (6). These formulas are mainly derived by calculating the power error caused by the current flowing in the capacitors. The worst case values of the relevant parameters in this work are listed in Table I together with the expected error in Table II. No significant error is expected in this work.

$$\left|\frac{\Delta P}{P}\right|_{C_{\mathrm{w,ref}}} \approx \frac{R_{\mathrm{Fe,DUT}} C_{\mathrm{w,ref}}}{k L_{\mathrm{m,DUT}}^2} \left(R_{\mathrm{s,ref}} L_{\mathrm{p,ref}} + R_{\mathrm{p,ref}} L_{\mathrm{s,ref}}\right) \tag{4}$$

$$\left|\frac{\Delta P}{P}\right|_{C_{\mathrm{s,ref}}} \approx -\frac{C_{\mathrm{s,ref}} + C_{\mathrm{diff}}}{k} \left(\frac{R_{\mathrm{p,ref}} R_{\mathrm{Fe,DUT}}}{L_{\mathrm{m,DUT}}} + \omega^2 L_{\mathrm{p,ref}}\right) \tag{5}$$

$$\left|\frac{\Delta P}{P}\right|_{C_{\mathrm{diff}}} \approx C_{\mathrm{diff}} \left(\frac{R_{\mathrm{s,DUT}} R_{\mathrm{Fe,DUT}}}{L_{\mathrm{m,DUT}}} + \omega^2 L_{\mathrm{s,DUT}}\right) \tag{6}$$

Table I: Parasitic components considered for error calculation

Parameters	Value
C_{diff}	2.75 pF
$C_{\mathrm{w,ref}}$	65 pF
$C_{\mathrm{p,ref}}$,$C_{\mathrm{s,ref}}$	8 pF
$R_{\mathrm{p,ref}}$,$R_{\mathrm{s,ref}}$	200 mΩ
$L_{\mathrm{p,ref}}$,$L_{\mathrm{s,ref}}$	38 nH
$R_{\mathrm{p,DUT}}$,$R_{\mathrm{s,DUT}}$	200 mΩ
$L_{\mathrm{p,DUT}}$,$L_{\mathrm{s,DUT}}$	35 nH
$L_{\mathrm{m,DUT}}$	486 nH
$R_{\mathrm{Fe,DUT}}$	250 Ω
ω	$2 \cdot \pi \cdot 30$ MHz
k	0.8

Table II: Calculated errors due to parasitic capacitances

Parameters	Value
$\left\|\frac{\Delta P}{P}\right\|_{C_{\mathrm{w,ref}}}$	1.3 %
$\left\|\frac{\Delta P}{P}\right\|_{C_{\mathrm{s,ref}}}$	1.6 %
$\left\|\frac{\Delta P}{P}\right\|_{C_{\mathrm{diff}}}$	3 %

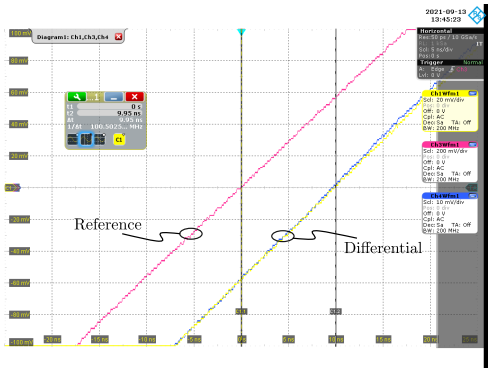

Fig. 2: Voltage measurement comparison: passive probe (reference) and two differential probes. About 10 ns time delay is observed while the gradient is identical.

Current Measurement

Current sensing is a critical part of the measurement system. Shunt resistor is chosen over current probe mainly due to the DC current measuring capability. The shunt resistor needs to have high precision with low stray inductance. Metal foil chip resistor from Susumu PRL series is used in this work. The shunt resistor has $R_{\text{sense}} = 0.1\ \Omega$ and $L_{\text{sense}} = 1\ nH$ as the nominal values, which is shown in Fig. 3. The shunt voltage is measured by the voltage probe, which brings the parasitic capacitance C_{probe}. Its nominal value is 9.5 pF for the RT-ZP10 from Rohde & Schwarz, which is used in this work. Passive probe can be used because the negative side is connected to ground. In addition, it provides high enough bandwidth, 200 MHz in this case.

The last step in current measurement is to transform the measured voltage into current. The stray inductance L_{sense} and voltage probe capacitance C_{probe} make the transformation less straightforward. The measured voltage v_{current} needs to be filtered by transfer function as shown in (7). The difference in measured voltage and calculated current is shown in Fig. 4. It can be seen that much smaller current is flowing through C_{probe}. This approach also anticipates the phase discrepancy brought by the shunt stray inductance.

$$i(s) = v_{\text{current}}(s)\left(\frac{1}{s \cdot L_{\text{sense}} + R_{\text{sense}}} + s \cdot C_{\text{probe}}\right) \tag{7}$$

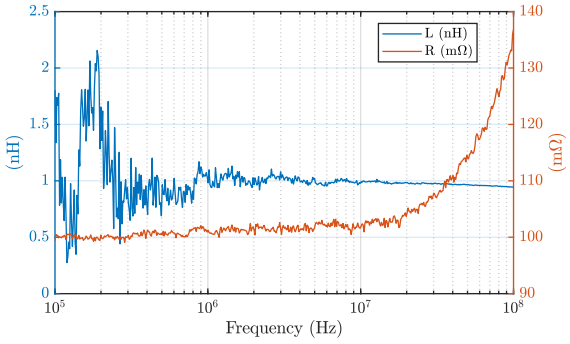

Fig. 3: Current shunt equivalent resistance and inductance

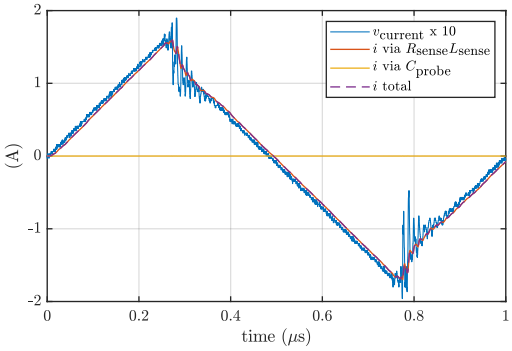

Fig. 4: Current measurement comparison: directly measured voltage and calculated current

Setup Verification

The setup is verified by testing toroid core under sine wave excitation. Then, the measurement results are compared with datasheet values. The measured cores are PC50 R22.1/13.7/7.9 and PC200 R15.8/8.9/4.7 from TDK. Fig. 5 shows the comparison result. The measurement point is given together with its uncertainty range, which is derived from 10 measurement captures. Measurement results match the datasheet values up to 1 MHz for PC50 material. However, for PC200 material, there is a discrepancy and the measurement gives higher losses than datasheet values. This discrepancy can happen in real practice [19], especially as the frequency goes higher. Nevertheless, the sine wave measurement results here can still be the basis for comparison in the next chapters.

3 Experimental Investigation

This work aims at measuring and analyzing core losses under square wave excitation from frequency of 500 kHz up to 3 MHz. The frequency range is motivated by state-of-the-art commercially available MnZn ferrite for power electronics application. The measurements were performed on two magnetic cores with different relative permeability (μ_{r}) level. They are listed in Table III along with their detailed properties. V_{e}, A_{e}, and l_{e} mean the magnetic core volume, effective cross section, and mean magnetic path length, respectively.

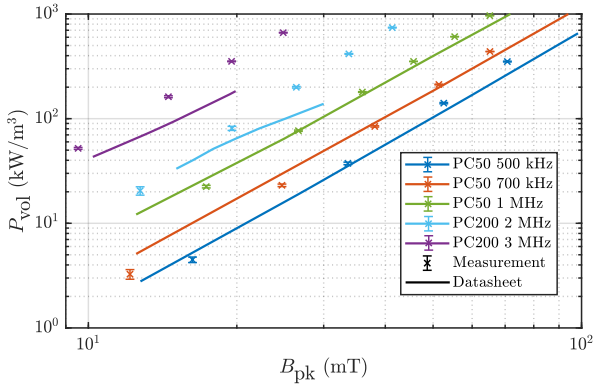

Fig. 5: Comparison between datasheet values and measurement results with sinusoid excitation

The measurement setup is discussed in the previous section and, in the end (2) and (3) are used to calculate the core losses. The magnetic flux density (B) is defined in Fig. 6 and can be calculated using (8) for the AC component and (9) for the DC component. Here N_s means the number of turns of sensing winding in the DUT and v_{DUT} is the sensed voltage. Care must be taken when calculating (3), due to the voltage overshoot at the edge of square wave. Voltage at the flat area of square wave is used to calculate (3) in this work.

$$B_{\mathrm{DUT}}(t) = \frac{1}{N_s \cdot A_e} \int_0^t v_{\mathrm{DUT}}(t)\, dt \tag{8}$$

$$H_{\mathrm{DC}} = \frac{N_{\mathrm{exc}} \cdot I_{\mathrm{DC}}}{l_e} \tag{10}$$

$$B_{\mathrm{DC}} = \mu_0 \cdot \mu_r \cdot H_{\mathrm{DC}} \tag{9}$$

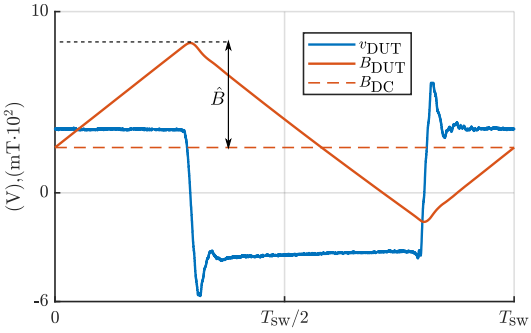

Fig. 6: Sensed DUT voltage (v_{DUT}) and the calculated flux density (B_{DUT}). This example is taken from core sample B at 1 MHz switching frequency

Table III: Core Under Test

Parameters	Core A	Core B
Core Material	PC50	PC200
Core Geometry	R 22.1/13.7/7.9	ER 14.5/6
V_e	1763 mm^3	334 mm^3
A_e	32.6 mm^2	17.6 mm^2
l_e	54.2 mm	19 mm
Initial μ_r	1500	800
B_{sat} at 25°C	490 mT	480 mT
Intended f_{sw}	0.3 - 1 Mhz	1 - 3 Mhz

Impact on Loss Curve

The first step to understand the effect of DC bias is to look at the loss curve. Fig. 7 and Fig. 8 show the losses density against peak AC flux density ($\hat{B}$) for core A and B, while Fig. 9 and Fig. 10 show the losses density against switching frequency. The diamond points in the figures are measurement points while the line is the result of regression.

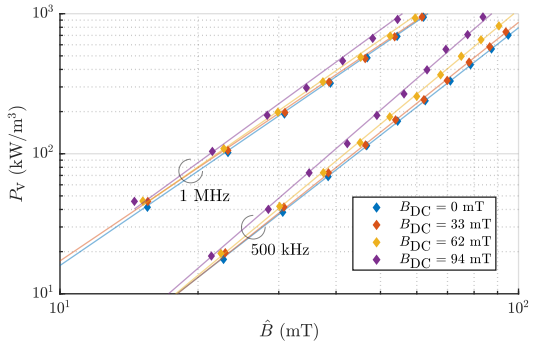

Fig. 7: Core losses density (P_v) versus flux density ($\hat{B}$) measured on test core A with different DC flux bias (B_{DC}) and frequency

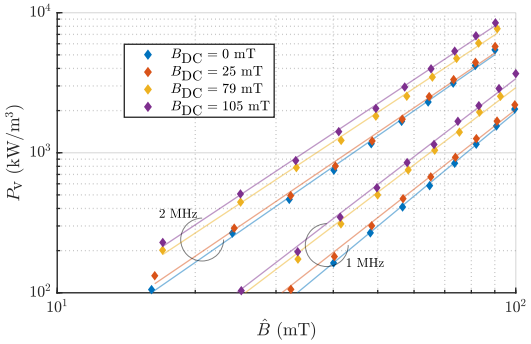

Fig. 8: Core losses (P_v) versus flux density ($\hat{B}$) measured on test core B with different DC flux bias (B_{DC}) and frequency

The influence of DC bias (B_{DC}) on P_v vs $\hat{B}$ can be seen in Fig. 7 and Fig. 8. At low DC bias the losses increase is relatively small. However, after the DC bias reaches a certain value, the losses increase starts to be significant. For example, at 500 kHz and $\hat{B} = 50mT$ in core A the losses increase at 33 mT bias is only 5.3 % but, at 62 mT bias the increase becomes 20 % and at 94 mT 51.4 %. For core B at 1 MHz and $\hat{B} = 50mT$ the trend is similar but at a different level. With 25 mT bias, the increase is 15.1 % but with 79 mT it becomes 75 %.

At a single frequency, the measured losses points still follow a straight regression line in logarithmic scale, even after DC bias is applied. This suggests that $P_v \propto \hat{B}^{\beta}$ relation still hold with DC bias. It is also observed that there is a slight shift in the regression line slope. This may suggest a shift in the β parameter. We also see this slope shift is less pronounced in core B, compared to core A. A more detailed modeling is presented in the later section.

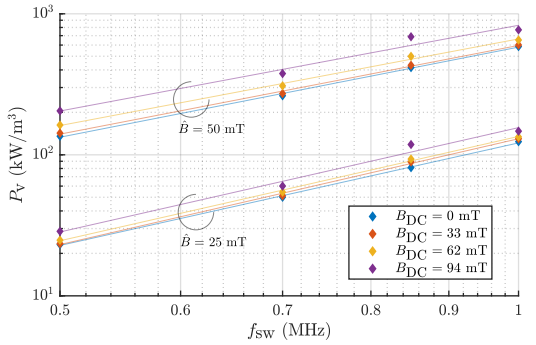

Fig. 9: Core losses (P_v) versus operating (switching) frequency (f_{sw}) measured on test core A with different DC flux bias (B_{DC}) and AC peak flux density ($\hat{B}$)

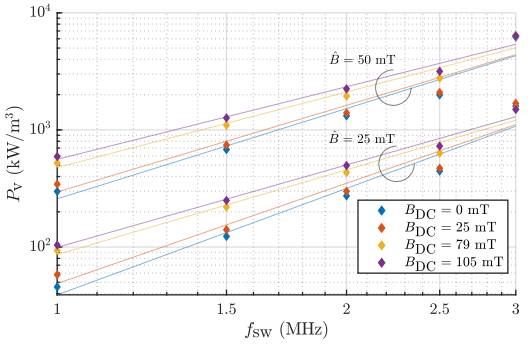

Fig. 10: Core losses (P_v) versus operating (switching) frequency (f_{sw}) measured on test core B with different DC flux bias (B_{DC}) and AC peak flux density ($\hat{B}$)

Fig. 9 and Fig. 10 show the influence of DC bias (B_{DC}) on P_v vs f_{sw} curve. A similar observation can be found where, again, at low DC bias the loss density increase is small. For test core A, the DC bias seems to offset the loss density curve, as in Fig. 9. Although not so clear, we can also see the $P_v \propto f_{sw}^{\alpha}$ relation and the shift in α parameter is not likely for core A. Meanwhile for core B, the relationship is less straightforward. The DC bias not only offsets the curve, but also changes the slope. In particular at $f_{sw} > 2$MHz, the effect becomes less predictable. At 3 MHz, the loss increase is almost unnoticeable. This can be caused by an error in the measurement system or it is a newfound characteristic of the magnetic core.

Relative Core Loss Increase

This subsection tried to answer when the DC bias starts to have important effect to the core losses. It is also chosen to quantify the DC bias using B field instead of H field. This selection enables magnetic core

performance comparison across different permeability value. The relative core losses increase ($P_{\text{v,rel}}$) is found by dividing the losses at a certain DC bias with the losses at no bias condition.

Figure 11 shows for core A when the DC bias impact becomes significant. The sum of AC and DC component of B field is taken as the X axis to show if there is relation between peak flux density and losses increase. The increase starts to become important, e.g more than 20 %, when the total B is above 100 mT. This can be seen by looking at the measurement points upper envelope. However, for $B_{\text{DC}} < 50$ mT, the increase stays low even when the sum is above 100 mT. It means the bias magnitude also plays a role in determining the increase. Furthermore, different operating frequency brings different impact. The higher frequency seems to create lower relative increase, as can be seen by comparing 1 MHz and 500 kHz points.

In test core B the trend and relationship is less straightforward. Figure 12 shows the relation between total B field and the relative losses increase. The measurement points are more widespread than core A. Contrary to core A behaviour, the relative loss increase is lower as the total flux increases, for a certain B_{DC}. This trend applies to all tested frequency and DC bias for core B. The DC bias magnitude also determines the relative increase and here the loss gain is more pronounced, e.g. at 1 MHz the $P_{\text{v,rel}}$ is close to two when $\hat{B} + B_{\text{DC}}$ is around 100 mT and $B_{\text{DC}} = 78$ mT. This is a steep increase and designers should take care of it when designing the magnetic components. Meanwhile, the impact of frequency is quite similar to core A. The higher frequency creates a lower relative loss increase.

The same data in Fig. 12 can also be presented in a different way as in Fig. 13. The B ratio of AC and DC components is plotted against loss increase. This is done to check if a different characteristics of the core losses can be seen. Nevertheless, a similar observation is found. The B_{DC} is the main controlling factor for $P_{\text{v,rel}}$. The B ratio plays a smaller role, although still has an impact, i.e. higher ratio makes lower loss increase. This observation reflects a complex physics behind the core losses phenomenon.

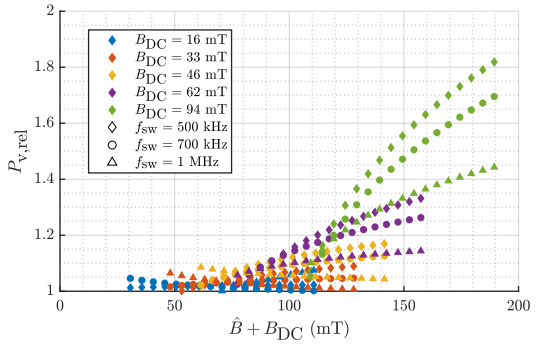

Fig. 11: Relative core losses ($P_{\text{v,rel}}$) versus peak total flux density ($\hat{B} + B_{\text{DC}}$) at different DC bias and frequency for test core A

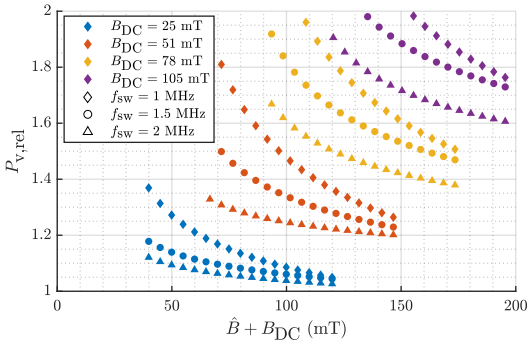

Fig. 12: Relative core losses ($P_{\text{v,rel}}$) versus peak total flux density ($\hat{B} + B_{\text{DC}}$) at different DC bias and frequency for test core B

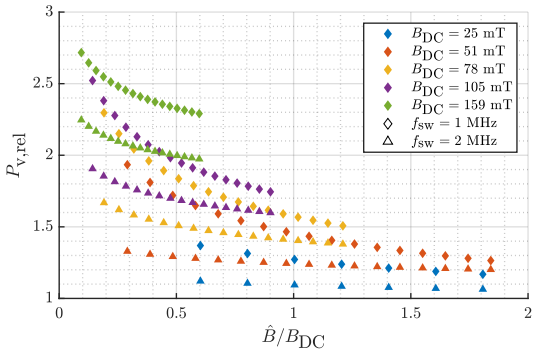

Fig. 13: Relative core losses ($P_{\text{v,rel}}$) versus flux density ratio ($\hat{B}/B_{\text{DC}}$) at different DC bias and frequency for test core B

4 Core Losses Modeling

This section does not try to propose a new model to predict core losses. Instead, we will see if the available models can still accurately predict core losses from the measurement results generated in this work, particularly this means incorporating the impact of DC bias on core losses. Out of many previously proposed core losses modeling [2, 4, 12, 15], the method in [12] will be used in the following analysis.

Analytical: iGSE with SPG

The main advantage of using analytical formula in modeling core losses is getting the insight into the physics behind the losses mechanism. The explicit formula shows the user which parameters are affecting the core losses. Hence, giving some understanding of the core losses behaviour.

Since in power electronics the flux (B) waveform is commonly not sinusoidal, the established improved Generalized Steinmetz Equation (*iGSE*) method [4] is adopted to calculate the core losses. However, this modeling does not include DC bias effect. Therefore, it needs to be modified with other techniques. The Steinmetz Premagnetization Graph (*SPG*) method [12] can incorporate the DC bias effect without changing the original equation so, it is used in this work. The iGSE formula when applied to triangular flux waveform is reduced to the form in (11). Then, with SPG, the α, β, and k_i will be modified following (12) which incorporates the dependency on DC bias B_DC.

The appropriate coefficients of SPG matrix (first term of right hand side in (12)) needs to be found in order to extract the dependency. This is done by solving an optimization or curve fitting problem. A least square algorithm has been implemented that fits calculated curve with measured data by minimizing the relative error. Despite the 4$^{\text{th}}$ order polynomial used here, the order can be varied if the optimization / curve fitting result does not generate a good prediction accuracy. In this work, the 4$^{\text{th}}$ order proves to be sufficient.

$$P_{\mathrm{v,iGSE,tri}} = k_\mathrm{i} \cdot (2f)^{\alpha} \cdot (\Delta B)^{\beta} \tag{11}$$

$$\begin{bmatrix} \alpha \\ \beta \\ k_\mathrm{i} \end{bmatrix} = \begin{bmatrix} \alpha_0 & 0 & 0 & 0 & 0 \\ \beta_0 & p_{\beta 1} & p_{\beta 2} & p_{\beta 3} & p_{\beta 4} \\ k_{\mathrm{i}0} & p_{ki1} & p_{ki2} & p_{ki3} & p_{ki4} \end{bmatrix} \cdot \begin{bmatrix} 1 \\ B_\mathrm{DC} \\ B_\mathrm{DC}^2 \\ B_\mathrm{DC}^3 \\ B_\mathrm{DC}^4 \end{bmatrix} \tag{12}$$

Following the mentioned procedure, the SPG dependency graph can be obtained. This is shown in Fig. 14 and Fig. 15 for core A and B, respectively. The data points are measurement result and the line is curve-fitting result. For core A, the α and β parameters stay relatively constant over the whole B_DC range. Meanwhile, k_i fluctuates smoothly at low B_DC and increases quite steeply after $B_\mathrm{DC} > 50$ mT. This observation aligns with the analysis in section 3, where the relative losses gain rises quickly after a certain B_DC values. For core B, the k_i increases steadily from low B_DC and shows an almost linear relation to B_DC. The β parameters has a slight decline from low to mid B_DC, while α shows a decreasing trend towards higher B_DC. The SPG prediction cannot capture the α shift because (12) assumes a constant α value. This assumption may not hold true anymore after seeing the measurement result in Fig. 12 and 13. Therefore, the modification of (12) is foreseen. Nevertheless, here the original SPG formulation is kept for the sake on consistency with previous works.

After having the SPG coefficients matrix, (11) is used to calculate the core losses in the presence of DC bias. The results are shown in Fig. 16 and Fig. 17 for core A and B, respectively, with several different $\hat{B}$ and f_sw values. The measurement points are also shown to compare the loss prediction and measurement. The iGSE + SPG method appears to be reasonably accurate in the whole B_DC range for

core A. The accuracy at low $\hat{B}$ (30 mT) is better than at high $\hat{B}$ (60 mT). For core B, this method loses accuracy at high $\hat{B}$ and high f_{sw}, as can be seen in Fig. 17. Nonetheless, the SPG enables losses prediction with DC bias.

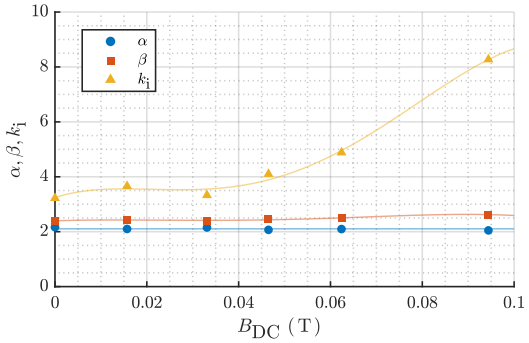

Fig. 14: Steinmetz Pre-magnetization Graph for test core A. The k_i value is scaled down by 10^4 to increase graph readability. The data points are measurement result and the line is curve-fitting result.

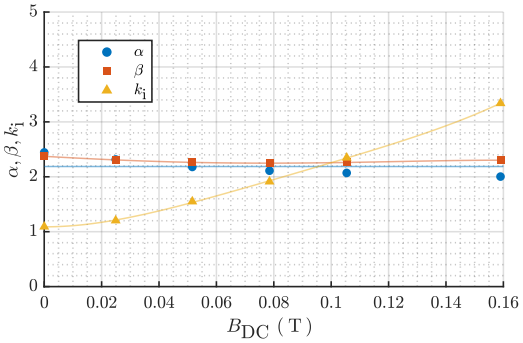

Fig. 15: Steinmetz Pre-magnetization Graph for test core B. The k_i value is scaled down by 10^4 to increase graph readability. The data points are measurement result and the line is curve-fitting result.

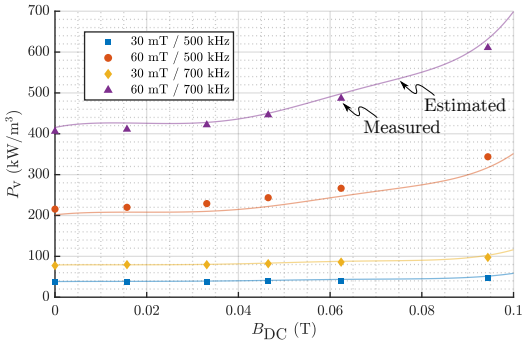

Fig. 16: Core loss density (P_v) estimation of test core A. The scatter points are measurement data while the curves are prediction result.

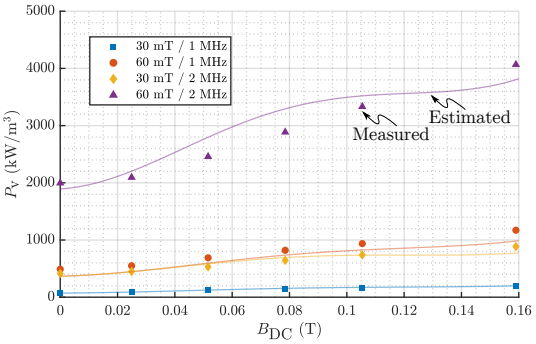

Fig. 17: Core loss density (P_v) estimation of test core B. The scatter points are measurement data while the curves are prediction result.

5 Conclusion and Future Work

This paper investigates magnetic core losses under square wave excitation with superimposed DC bias. The frequency of interest is from 500 kHz up to 3 MHz and the tested material is MnZn ferrite with nominal relative permeability (μ_r) of 1500 and 800 which are the state-of-the-art for power electronics application. Chapter 2 describes the core losses measurement setup. The mutual inductance neutralization method is used to minimize the measurement error. The measurement results are presented in chapter 3. The DC bias basically generates an offset to the loss curve, creating higher losses. It was also seen that there is a shift in Steinmetz parameter, especially β, after bias is applied. Nevertheless, the proportionality $P_v \propto \hat{B}^{\beta}$ and $P_v \propto f_{sw}^{\alpha}$ still hold. Chapter 4 attempts to model the core losses behaviour by using the combined approach: Steinmetz Premagnetization Graph (SPG) with iGSE. This method modifies the Steinmetz parameter using a polynomial function of the DC bias and the model generates a maximum error percentage of 25% in our test. In summary, this paper clarifies ferrite core losses behaviour in the mentioned frequency range under DC bias, and quantitatively analyzes the possible models. As a further step, the models and measurement data can be expanded and shared to be used with other magnetic designers.

REFERENCES

[1] I. D. Mayergoyz and G. Friedman, "Generalized Preisach model of hysteresis," *IEEE Transactions on Magnetics*, vol. 24, no. 1, pp. 212–217, 1988.

[2] M. Albach, T. Durbaum, and A. Brockmeyer, "Calculating core losses in transformers for arbitrary magnetizing currents a comparison of different approaches," in *PESC Record. 27th Annual IEEE Power Electronics Specialists Conference*. IEEE, 1996.

[3] J. Reinert, A. Brockmeyer, and R. De Doncker, "Calculation of losses in ferro- and ferrimagnetic materials based on the modified Steinmetz equation," *IEEE Transactions on Industry Applications*, vol. 37, no. 4, 2001.

[4] K. Venkatachalam, C. Sullivan, T. Abdallah, and H. Tacca, "Accurate prediction of ferrite core loss with nonsinusoidal waveforms using only Steinmetz parameters," in *2002 IEEE Workshop on Computers in Power Electronics, 2002. Proceedings.* IEEE, 2002.

[5] W. Roshen, "Ferrite core loss for power magnetic components design," *IEEE Transactions on Magnetics*, vol. 27, no. 6, 11 1991.

[6] W. A. Roshen, "A Practical, Accurate and Very General Core Loss Model for Nonsinusoidal Waveforms," *IEEE Transactions on Power Electronics*, vol. 22, no. 1, pp. 30–40, 2007.

[7] P. Papamanolis, T. Guillod, F. Krismer, and J. W. Kolar, "Transient Calorimetric Measurement of Ferrite Core Losses up to 50 MHz," *IEEE Transactions on Power Electronics*, vol. 36, no. 3, 3 2021.

[8] Jieli Li, T. Abdallah, and C. Sullivan, "Improved calculation of core loss with nonsinusoidal waveforms," in *Conference Record of the 2001 IEEE Industry Applications Conference. 36th IAS Annual Meeting (Cat. No.01CH37248)*. IEEE, 2001.

[9] A. Van den Bossche, V. Valchev, and G. Georgiev, "Measurement and loss model of ferrites with non-sinusoidal waveforms," in *2004 IEEE 35th Annual Power Electronics Specialists Conference (IEEE Cat. No.04CH37551)*. IEEE, 2004.

[10] W. G. Hurley, T. Merkin, and M. Duffy, "The Performance Factor for Magnetic Materials Revisited: The Effect of Core Losses on the Selection of Core Size in Transformers," *IEEE Power Electronics Magazine*, vol. 5, no. 3, 9 2018.

[11] A. Brockmeyer, "Experimental evaluation of the influence of DC-premagnetization on the properties of power electronic ferrites," in *Proceedings of Applied Power Electronics Conference. APEC '96*. IEEE, 1996.

[12] J. Muhlethaler, J. Biela, J. W. Kolar, and A. Ecklebe, "Core Losses Under the DC Bias Condition Based on Steinmetz Parameters," *IEEE Transactions on Power Electronics*, vol. 27, no. 2, 2 2012.

[13] A. J. Hanson, J. A. Belk, S. Lim, C. R. Sullivan, and D. J. Perreault, "Measurements and Performance Factor Comparisons of Magnetic Materials at High Frequency," *IEEE Transactions on Power Electronics*, vol. 31, no. 11, 11 2016.

[14] D. Hou, M. Mu, F. C. Lee, and Q. Li, "New high-frequency core loss measurement method with partial cancellation concept," *IEEE Transactions on Power Electronics*, vol. 32, no. 4, pp. 2987–2994, 4 2017.

[15] E. Stenglein and T. Durbaum, "Core Loss Model for Arbitrary Excitations With DC Bias Covering a Wide Frequency Range," *IEEE Transactions on Magnetics*, vol. 57, no. 6, 6 2021.

[16] F. Dong Tan, J. Vollin, and S. Cuk, "A practical approach for magnetic core-loss characterization," *IEEE Transactions on Power Electronics*, vol. 10, no. 2, 3 1995.

[17] C. Baguley, U. Madawala, and B. Carsten, "A New Technique for Measuring Ferrite Core Loss Under DC Bias Conditions," *IEEE Transactions on Magnetics*, vol. 44, no. 11, 11 2008.

[18] M. Mu, Q. Li, D. J. Gilham, F. C. Lee, and K. D. Ngo, "New core loss measurement method for high-frequency magnetic materials," *IEEE Transactions on Power Electronics*, vol. 29, no. 8, pp. 4374–4381, 2014.

[19] P. Papamanolis, T. Guillod, F. Krismer, and J. W. Kolar, "Minimum Loss Operation and Optimal Design of High-Frequency Inductors for Defined Core and Litz Wire," *IEEE Open Journal of Power Electronics*, vol. 1, 2020.